Twitching Control for Pneumatic Artificial Muscle Actuators

Piotr A. Bogdan[1], Oliver Smith[1], Frederico B. Klein[1], Mario Gianni[2]

***Abstract*— In this work we present the design and development of a twitching control system for pneumatic artificial muscle (PAM) actuators. In this system, a shape memory alloy (SMA) poppet valve is used to control the flow of air pressurizing the inner bladder of a McKibben-based PAM. The valve is driven by pulse width modulation with changing frequency, allowing the PAM to resemble the mammalian muscles twitching. An adjustable passive exhaust orifice is used in place of an exhaust air valve to release the air pressure from the bladder mimicking natural muscle relaxation behaviour. Experiments under isometric and isotonic contractions show that the proposed control system reduces hysteresis of about 72% compared to continuous activation against 15% loss in contraction force with respect to conventional exhaust air valves.**

I. Introduction

In the last decade, the use of Pneumatic Artificial Muscles (PAMs) in biorobotic [1]–[3], medical [4]–[8] and industrial applications [9]–[11] has significantly increased. Compared to conventional actuating mechanisms, such as hydraulic actuators, electric motors and pneumatic pistons, PAMs can provide a higher power-to-weight ratio [12]. They can exhibit more flexible and compliant behaviours under low output impedance [13]. PAMs can also be used in a variable stiffness configuration [14]. Moreover, they can mimic human-like muscular functions [15].

PAMs are contractile and linear motion actuators made of an elastomeric bladder enclosed in a braided mesh sleeve with two end-fittings that seal off both ends [16] (see Figure 1). The actuator is operated by the air pressure and depending on how the braided sleeve fibres are oriented, it either contracts or stretches axially in response to the air pressurising the bladder.

Valve design and actuation significantly affect the power-to-weight, the force-to-weight and the volume-to-weight ratios and thus the energy efficiency of PAM actuators [17]. Electromagnetic control valves, such as continuously acting servo-proportional and discrete on-off switching valves, are commonly used to regulate the flow rate and the air pressure in the bladder. Compared to their discrete counterpart, proportional valves allow for a more precise control of the flow. However, discrete on-off switching valves are less expensive, more compact and lightweight than proportional valves, making them better suited for cost-effective applications where low volume-to-weight is essential. Standard discrete on-off switching valves feature either a solenoid or a piezo element (i.e., electromechanical transducer). Piezoelectric valves are well-known to require less power than solenoid valves as they do not need any holding current to maintain a switched state. Nonetheless, the air flow rate enabled by these valves is much lower than the rate generated by the solenoid ones, limiting the use of piezoelectric valves to small-scale applications. To achieve the same performance of a solenoid valve in terms of flow rate while keeping the power consumption at minimum, the mass of the piezoelectric valve requires to be increased. However, this would negatively affect the volume-to-weight ratio of the actuator. Shape Memory Alloy (SMA) has been used as a lightweight and low power consumption alternative to solenoid and piezoelectric elements to actuate the valves [18]. SMAs have the ability to rapidly change shape when heated, enabling fast valve actuation. However, their operational frequency is limited by slow passive cooling [19].

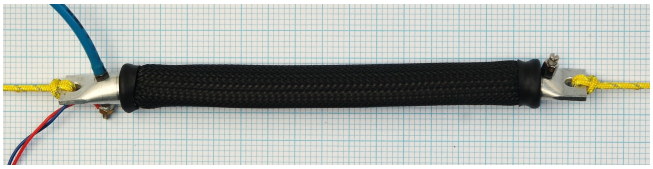

Fig. 1. Prototype of the SMA valve McKibben-based PAM with passive exhauste orifice.

Discrete on-off switching valves are commonly controlled by pulse width modulation (PWM) [20]. This control method has the main advantage of reducing the valve response time [21]. It can also reduce the non-linearity of the valves and the related dead-bands [22]. Moreover, when utilized to operate the valves, PWM can result in significant power saving and heat reduction while maintaining the desired proportional characteristics [23]. PWM-based control allows to regulate the airflow rate by adjusting the duty cycle of the signal [24]. However, the frequency of the signal also effects the dynamics of the actuator. Therefore, having an additional degree of freedom such as frequency modulation [25] would be helpful in PWM-based control to enable PAM to better mimic its biological counterpart.

In biology, muscle motor unit is the basic building block of mammalian muscles responding to motor neuron activation with a short contraction called muscle twitch. With frequent activations of a single motor unit, the isolated twitches start to overlap, creating a continued tetanic force profile with additional visible force ripple [26] [27].

In this work we present the design and development of a twitching control system for a SMA-Valve McKibben-based PAM with passive exhaust orifice. Similarly to [28],

[1]School of Engineering, Computing and Mathematics, Faculty of Science and Engineering, University of Plymouth, UK

[2]School of Electrical Engineering, Electronics and Computer Science, University of Liverpool, UK

Manuscript 385 submitted to 2023 IEEE International Conference on Robotics and Biomimetics (ROBIO). Received August 15, 2023.

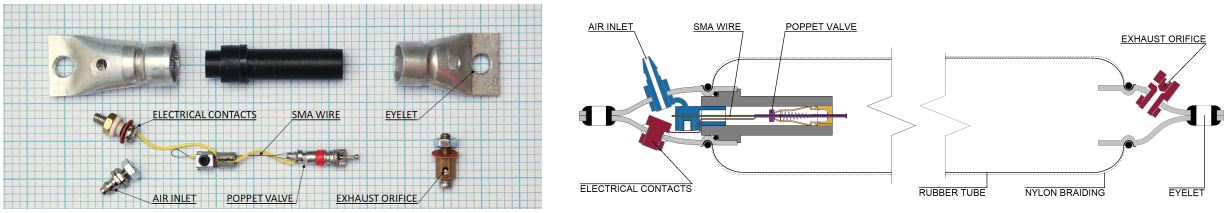

(a) (b)

Fig. 2. (a) Components of the PAM; (b) Cross section of the PAM.

a popped valve incorporated into the muscle end-cap has been used to increase the airflow rate and to reduce the mass. However, a passive exhaust orifice instead of a second poppet valve has been located in the opposite end-cap to allow the air release from the bladder to the atmosphere. The stem of the popped valve is actuated by a lightweight nickel-titanium (NiTi) SMA wire. Compared to solenoid and piezoelectric valves, this valve enables faster PWM-based switching control due to its purely resistive impedance. Frequency modulation has been used with PWM to control the force ripple in order to better generate force profiles similar to those found in muscle motor units. The SMA-Valve McKibben-based PAM actuated by the frequency modulated PWM signal and featuring the passive exhaust orifice is capable of mimicking mammalian muscles twitching and natural relaxation behaviours.

The paper is organized as follows. Section II describes the design of the actuator and the twitching control strategy. Section III presents the isotonic and isotmetric experiments evaluating the efficiency, twitch response, useful working range, and reduction of hysteresis of the PAM. Conclusions in Section IV summarise the results.

II. Control System Design

Figure 3 illustrates the proposed design of the McKibben actuator.

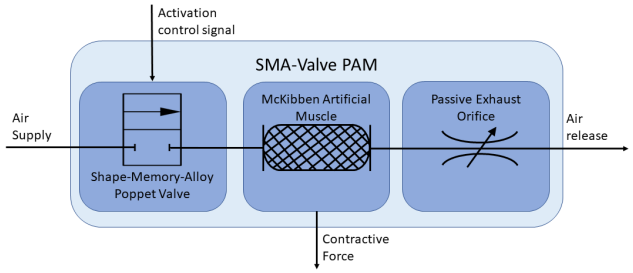

Fig. 3. Block diagram of the SMA valve McKibben PAM actuator.

The SMA valve is responsible for controlling the input flow of air used to pressurize the pneumatic bladder of the muscle. A standard poppet valve is modified by adding a 20mm length of 0.15mm diameter nickel-titanium (NiTi) shape memory alloy wire. When subjected to electrical current, the wire pulls on the poppet stem to open the valve. To cope with the slow passive heat dissipation required to close the valve, the latter has been housed within the air inlet. The air passing through the inlet when the valve is open is used to cool down the NiTi wire and, consequently, close the valve. This cooling mechanism enhances the SMA valve response (see experiments in Sub-section III-A).

A passive exhaust orifice has been used in place of an active exhaust valve to vent the bladder. When the SMA valve is open the passive exhaust orifice traps the air inside the bladder thus inflating the muscle. Conversely, when the SMA valve is closed, the orifice allows the airflow to naturally vent into the atmosphere. This throttling friction effect can be regulated by manually adjusting the aperture of the orifice via a screw. This feature enables bio-mimicry of fast contraction followed by of natural relaxation found in mammalian muscles force profile [29].

Two rigid end couplings have been made from 12mm crimped aluminum tube to seal both the ends of the pneumatic bladder, whilst functioning as eyelet anchor points for attachment, incorporating the electrical contacts of the SMA valve, and both the air inlet and the passive exhaust orifice (see Figure 2). Table I reports the physical parameters of the constructed McKibben PAM.

TABLE I
Physical Parameters of the SMA-Valve PAM Actuator

Weight	Valve	End couplings	Total
	5g	5g	25g
Dimensions	Total length	Bladder length	Diameter
	19cm	14cm	2cm
Stroke	Unloaded	Loaded with 2kg	Loaded with 10kg
	25mm	21mm	10mm

The SMA valve is actuated by a control signal $u(t)$, with $t = 0, \ldots, T$ (see Eq. 1). This control signal is generated by combining together a pulse width modulation (PWM) signal $u_{\text{PWM}}(t)$ (see Eq. 2) and a pulse density modulation (PDM) signal $u_{\text{PDM}}(t)$ (see Eq. 3). A representation of these two signals can be seen in Figure 4.

$$u(t) = u_{\text{PWM}}(t) \cdot u_{\text{PDM}}(t) \tag{1}$$

$$u_{\text{PWM}}(t) = \begin{cases} 1 & \text{if } t - t_c \cdot \left\lfloor \dfrac{t}{t_c} \right\rfloor < t_d \\ 0 & \text{otherwise} \end{cases} \tag{2}$$

Manuscript 385 submitted to 2023 IEEE International Conference on Robotics and Biomimetics (ROBIO). Received August 15, 2023.

$$u_{\text{PDM}}(t) = \begin{cases} 1 & \text{if } t - t_a \cdot \left\lfloor \frac{t}{t_a} \right\rfloor < t_p \\ 0 & \text{otherwise} \end{cases} \quad (3)$$

Here t_c and t_d are the period and width of $u_{\text{PWM}}(t)$ while t_a and t_p are the period and width of $u_{\text{PDM}}(t)$, with $t_c \ll t_p$. Also, while t_c and t_p are constants, $t_d^{min} \leq t_d \leq t_d^{max}$ and $t_a^{min} \leq t_a \leq t_a^{max}$.

Varying the duty cycle t_d/t_c of the $u_{\text{PWM}}(t)$ signal allows to control the instantaneous power applied to the SMA valve. On the other hand, by keeping constant the width t_p of the $u_{\text{PDM}}(t)$ signal is possible to maintain the period of power transfer constant while by varying its frequency $1/t_a$, the valve activation frequency can be controlled. As the period of power transfer can also affect the valve efficiency and timing, the designed control signal allows to limit potential unknown effects throughout the experiments.

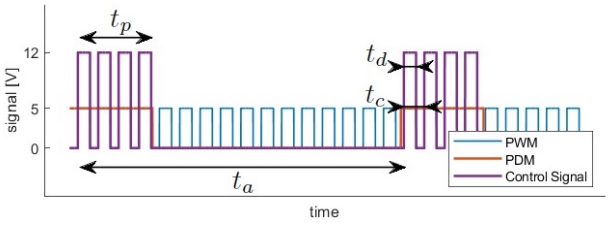

Fig. 4. Shape of the control signal in Eq. 1 applied to the SMA valve. The short and constant bursts of pulses repeated over longer and variable periods creates pulse density modulation (PDM) mixed with fast power dosing pulse width modulation (PWM) signal.

III. Experiments

In this section we describe the experiments conducted to evaluate the performance of the SMA-Valve PAM with the passive exhaust orifice under both isometric (i.e., constant length, variable force) and isotonic (i.e., constant force, variable length) conditions. For this purpose a test rig has been constructed (see Figure 5). The rig is made of a sturdy wooden frame hosting a 3D printed pulley for isotonic contractions and an adjustable contraction limiter for isometric contractions.

A single point load cell sensor (Tedea-Huntleigh model 1241) with 32bit resolution analogue-to-digital converter (Texas Instruments ADS1262) sampling at 1200Hz has been used to measure forces while a hall-effect position sensor (Broadcom AEAT-6012-A06) with 12bit resolution at 500Hz has been used to measure the change in length during isotonic contractions. Based on the stroke length of the PAM and the corresponding angular range of the pulley (see Table I), a 5-to-1 gear reduction has been added to increase the resolution of the position sensor. A electronic switch powered by 12V has been used to control the valve. The valve is activated by the control signal in Eq. 1 generated by a micro-controller unit. In all the experiments the air pressure supplied to the muscle has been kept constant at 0.2MPa. Moreover the period t_c of the PWM signal $u_{\text{PWM}}(t)$ (see Eq. 2) and the width t_p of the PDM signal $u_{\text{PDM}}(t)$ (see Eq. 3) have been set equal to 16μs and 10ms, respectively. $t_c = 16\mu$s corresponds to the minimum period at which the micro-controller unit can generate the control signal. $t_p = 10$ms has been experimentally determined as a trade-off between the activation period and the power consumption of the valve.

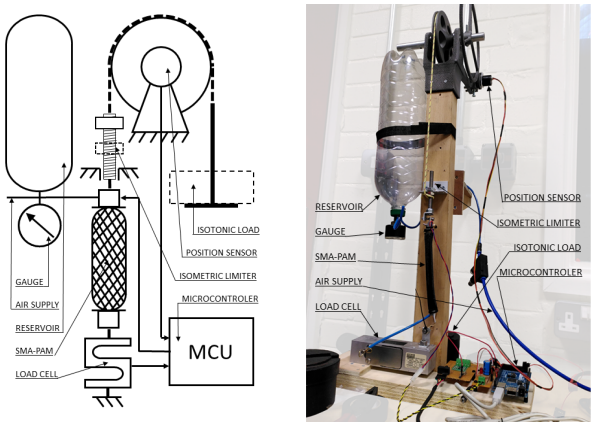

(a) Diagram of the test rig (b) Photo of the test rig

Fig. 5. Experimental test rig, featuring the PAM, load cell, 3D printed pulley and position sensor. A detailed diagram 5a and a photo 5b.

A. Natural energy expenditure with a passive exhaust orifice

The main purpose of this experiment is to evaluate the effectiveness of the passive exhaust orifice in enabling the SMA-Valve PAM to re-create a twitch similar to the one in the mammalian muscles [29]. For this purpose, we measure the twitch force profile under isometric contractions for different apertures of the passive exhaust orifice. To this end, the contraction ratio of the muscle has been kept fixed at 50%. The period t_a and the width t_d of the PDM signal $u_{\text{PDM}}(t)$ (see Eq. 3) have been set equal to 2s and 10ms, respectively. The duty cycle t_d/t_c of the PWM signal $u_{\text{PWM}}(t)$ (see Eq. 2) has been set equal to 32%. Four different settings of the passive exhaust orifice have been considered, namely, $0.0T$ (fully closed), $0.1T$, $0.3T$ and $2.0T$, with T representing the number of screw turns. Under this setting, the twitch force profile has been recorded over 30 activations for each configuration of the passive exhaust orifice. In the configuration where the orifice is fully closed, the muscle has been manually emptied after each activation.

Figure 6 shows the mean and the standard deviation of the twitch force profile for each configuration of the passive exhaust orifice. Here, the profiles have been aligned according to the activation signal and the twitch force profile with the passive exhaust orifice in fully closed configuration has been considered as a baseline for the comparison. In all the orifice configurations it can be noted that the valve opens after less than 0.1s from the activation signal (see Figure 6). Under the $0.1T$ configuration of the orifice, the twitch force reaches almost 85% of the maximum value of the force which can be obtained when the orifice is fully

Manuscript 385 submitted to 2023 IEEE International Conference on Robotics and Biomimetics (ROBIO). Received August 15, 2023.

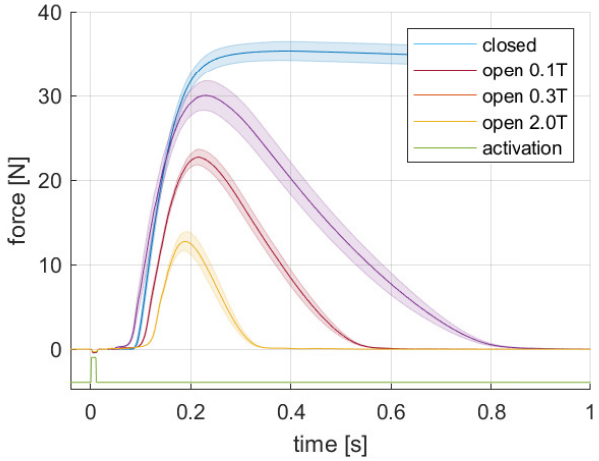

Fig. 6. Mean and standard deviation of the twitch force profile recorded over 30 activations for different configurations of the passive exhaust orifice. The activation signal in Eq. 1 not in scale is overlaid for timing reference.

closed. Moreover, the decay time is about 7 times longer than the peak time and the valve closes at 0.23s. At $0.3T$ the twitch force reaches 65% of the baseline with a decay time 3 times longer than the peak time with the valve closing at 0.22s. Finally, when the orifice is opened at $2.0T$ the twitch force reaches 35% of the baseline and the decay and peak times are almost equivalent. In this configuration, the valve closes at 0.19s.

These results demonstrate that although the SMA-Valve can open at high speed, it restrict the air flow into the muscle as it can be seen from the slope of the twitch force profile. A similar throttling effected is generated by the passive exhaust orifice, as it can be observed from the twitch force profile decay. However, by keeping high the ratio between the peak and the decay times the loss of twitch force can be limited. Finally, the twitch force profile obtained in the experiment shows that the SMA-Valve in combination with the passive exhaust orifice allows for mimicking the mammalian muscle twitching behaviour as illustrated in [29].

B. Power efficiency gains with a twitching activation signal

The main purpose of this experiment is to validate under isometric conditions the hypothesis that the proposed control signal in Eq. 1 is more efficient in opening the SMA-Valve than continuous activation with respect to power consumption while generating the same contraction force. This is due to the valve being powered for short periods of time while closing which is more efficient in terms of heating, rather than continuously maintaining the opening state. The power consumption of the SMA-Valve can be calculated as follows

$$P = \frac{E}{t_a} \quad \text{with} \quad E = \frac{t_p t_d V^2}{t_c R} \tag{4}$$

where E is the energy required to activate the valve, V is the supply voltage and R is the valve combined resistance. Here, $V = 12$V and $R = 660$mOhm. The contraction ratio of the muscle has been set equal to 50%. Three different values for the frequency $1/t_a$ of the PDM signal $u_{\text{PDM}}(t)$ (see Eq. 3) have been considered, namely, 3.5Hz, 10Hz, 16Hz, including continuous activation. The latter is obtained by setting $t_a = t_p$. For each value of the frequency, the duty cycle t_d/t_c of the PWM signal $u_{\text{PWM}}(t)$ (see Eq. 2) has been experimentally estimated such that the muscle contracted with resulting force of 15N. This value has been chosen to reduce at minimum the non-linear characteristic between the proposed control signal and the generated contraction force (see experiment in Sub-section III-C). Under this setting, five contractions of 30s each have been performed for each frequency of the PDM signal $u_{\text{PDM}}(t)$ (see Eq. 3). Table II reports the average $\overline{P}$ of the valve power consumption, the average $\overline{E}$ of the energy required to actuate the valve, the average $\overline{F}_p$ and $\overline{F}_{p-p}$ of the peak and the peak-to-peak ripple force generated within the duration of the contraction, respectively, over the five contractions for each frequency value and the continuous case.

TABLE II

AVERAGES OF THE VALVE POWER CONSUMPTION, THE VALVE ENERGY ACTIVATION, THE PEAK AND THE PEAK-TO-PEAK RIPPLE FORCES OVER THE FIVE CONTRACTIONS FOR EACH FREQUENCY VALUE, INCLUDING THE CONTINUOUS CASE

$1/t_a$[Hz]	t_d/t_c[%]	$\overline{P}$[W]	$\overline{E}$[J]	$\overline{F}_p$[N]	$\overline{F}_{p-p}$[N]
3.5	12.9	1.0	0.28	14.6	12.8
10	7.8	1.7	0.17	21.3	1.9
16	5.9	2.0	0.13	15.9	0.8
Cont	1.65	3.6	N/A	13.1	0.5

The values in the third column of Table II show that the power consumption is reduced when the valve is activated by the proposed control signal. Under 10Hz and a PWM duty cycle of 7.8%, the valves requires half of the power with respect to the continuous case also generating a higher peak force. However, as it can be noted in the fifth column of Table II, controlling the valve using the proposed control signal introduces a peak-to-peak force variation effect similar to mammalian muscles [26] [30]. Unlike its biological counterpart, this peak-to-peak force variation can be controlled and it does not significantly increase compared to the continuous case. Note that the exact contraction force of 15N has not been reached by the estimated PWM duty cycle due to the open-loop control setting of the valve.

C. Useful working range under isotonic Contraction

This experiment has been designed to demonstrate under isotonic conditions the capability of the SMA-Valve actuator with the passive exhaust orifice to generate motion under a load. For this purpose, five different laboratory reference weights have been used, namely, 0.5Kg, 1Kg, 2Kg, 5Kg and 10Kg. Based on the results in Sub-section III-B, the frequency $1/t_a$ of the PDM signal $u_{\text{PDM}}(t)$ (see Eq. 3) has been set equal to 10Hz. Three different values for the duty cycle t_d/t_c of the PWM signal $u_{\text{PWM}}(t)$ (see Eq. 2) have been considered, namely, 5.9%, 7.8% and 9.8%. These values have been experimentally estimated and denote three

different contraction configurations in which the PAM has been set. These configurations are similar to the muscular contractions in response to the beginning of tetanic summation, unfused tetanus and fused tetanus. Five contractions of 20s have been performed for each reference weight and for each duty cycle. In each contraction, the displacement of the reference weight has been measured using the position sensor of the rig (see Figure 5) and the change in potential energy has been estimated. Figure 7 shows the mean and

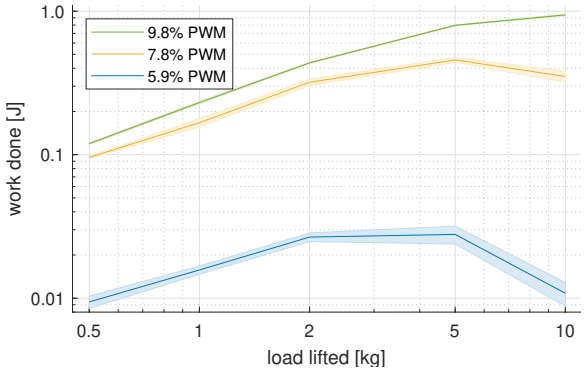

Fig. 7. Mean and standard deviation of the work done by the SMA-Valve PAM actuator with the passive exhaust orifice during isotonic contractions lifting different static loads at different duty cycles of the PWM signal $u_{\text{PWM}}(t)$ (see Eq. 2) over five trials.

the standard deviation of the work done on the different reference weights for each value of the duty cycle over the five contractions. From these results it can be noted that operating the muscle at a duty cycle of 5.9% is more efficient in terms of airflow rate when 2Kg of reference weight is considered. Better performance than 5.9% can be obtained at a duty cycle of 7.8% for 5Kg of reference weight. To perform work on a reference weight of 10Kg, a duty cycle of 9.8% is required. Likewise in mammalian muscle motors units a specific range of operation for the designed actuator can also be identified [30]. In this regard, 5.9%-9.8% represents the effective range of duty cycles. Within this interval, 2Kg-10Kg correspond to the most efficient range of reference weights.

D. Reducing hysteresis through pulse density modulation

In Sub-section III-B we observed that the proposed control signal $u(t)$ (see Eq. 1) introduces an additional degree of freedom which allows for adjusting the peak-to-peak force ripple of the contractive force. This property can have a significant impact also in reducing the hysteresis of the PAM's displacement. To demonstrate this effect an isotonic experiment has been designed as follows. Based on the results in Sub-section III-C 2Kg has been used as a reference weight. 3.5Hz has been selected for the frequency $1/t_a$ of the PDM signal $u_{\text{PDM}}(t)$ (see Eq. 3) to generated a significant peak-to-peak force ripple of the contractive force (see last column of Table II in Sub-section III-B). As for the experiments in Sub-section III-B this case has been

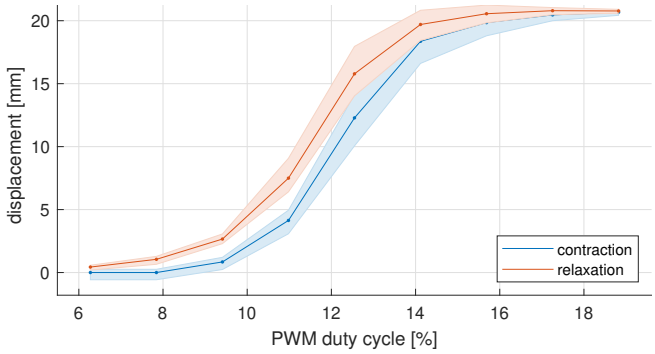

(a)

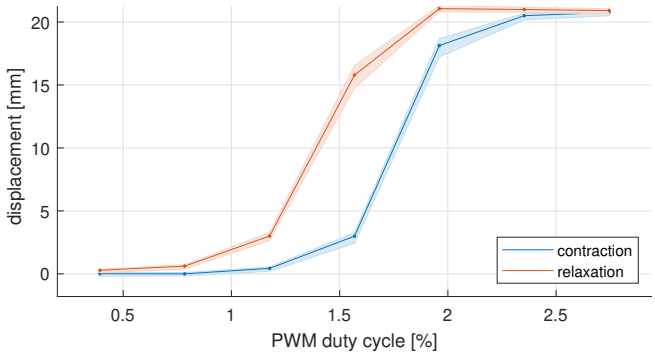

(b)

Fig. 8. Average of the measured hysteresis loops (lines) and average peak-to-peak displacement ripple (patches) ranging from full contraction to full relaxation under 2kg reference weight over 10 trials at: (a) 3.5Hz and (b) continuous activation .

compared with the case of continuous activation. 6.27%-18.8% with increments of 1.57% and 0.39%-2.75% with increments of 0.39% have been chosen for the range of duty cycles t_d/t_c of the PWM signal $u_{\text{PWM}}(t)$ (see Eq. 2) for the case of 3.5Hz and continuous activation, respectively. These ranges have been experimentally estimated to span from full relaxation to full contraction states of the muscle under the considered reference weight. 10 trials have been performed. In each trial the PAM has been controlled with the designated frequencies of the PDM signal $u_{\text{PDM}}(t)$ while cycling over the corresponding ranges of the duty cycles of the PWM signal $u_{\text{PWM}}(t)$. While cycling, each value of the duty cycle for each frequency was hold for 5s to stabilise the muscle and erase any rate-dependent hysteresis element. The last second was recorded for calculating the average displacement and peak-to-peak displacement ripple over the 10 trials. Figure 8 show the average of the measured hysteresis loops and the average peak-to-peak displacement ripple of the PAM at 3.5Hz and for the continuous activation case. Table III reports the difference $\Delta\overline{d}$ of the average displacement hysteresis $\overline{d}$, the average peak-to-peak displacement ripple $\overline{d}_{p-p}$, measured at the mid-points of the duty cycle ranges, for 3.5Hz and the continuous activation. Table III also reports the average stroke $\overline{s}$ and the ratio between the $\Delta\overline{d}$ and $\overline{s}$. As it can be noted in Table III, actuating the PAM using the proposed control signal introduces a slightly higher peak-to-peak displacement ripple while reducing the

TABLE III

DIFFERENCE OF THE AVERAGE DISPLACEMENT, AVERAGE PEAK-TO-PEAK DISPLACEMENT RIPPLE, AVERAGE STROKE AND THE RATIO BETWEEN THE AVERAGE DISPLACEMENT OFFSET AND AVERAGE STROKE FOR 3.5HZ AND THE CONTINUOUS ACTIVATION

$1/t_a$	$\Delta\overline{d}$[mm]	$\overline{d}_{p-p}$[mm]	$\overline{s}$[mm]	$\Delta\overline{d}/\overline{s}$[%]
3.5Hz	3.5	4.0	20.9	16.7
Cont	12.8	1.8	20.9	61.2

displacement hysteresis by 72% from 12.8mm to 3.5mm. Moreover, compared to 3.5Hz, in the continuous activation case the ratio between the $\Delta\overline{d}$ and $\overline{s}$ is higher than half of the muscle stroke making it more difficult to control without close-loop feedback.

IV. CONCLUSIONS

In this paper we described the design and development of a McKibben actuator. A Nitinol SMA valve located in the end-cap is used to supply the actuator with air. A passive exhaust orfice in the opposite end-cap allows for air release from the bladder. The SMA valve is controlled by a frequency modulated PWM signal which regulates the airflow rate into the bladder and also the profile of the contractive force. Experiments under isometric conditions have shown that the SMA valve in combination with the passive exhaust orifice allows for mimicking the mammalian muscle single twitch force profile. Twitch force profiles with different characteristics can be obtained under different settings of the passive exhaust orifice. For isometric contractions, operating the SMA valve with the proposed frequency modulated PWM signal results in significant reduction of power consumption while providing an additional degree of freedom to control the force ripple. Our experiments under isotonic conditions have shown that this feature also enabled PAM to significantly reduce hysteresis in open-loop control.

In conclusion, the proposed frequency modulated PWM-driven PAM can provide flexible and compliant control for application where a more accurate bio-mimicry of mammalian muscles is required.

REFERENCES

[1] K. Hosoda *et al.*, "Pneumatic-driven jumping robot with anthropomorphic muscular skeleton structure," *Auton. Robots*, vol. 28, pp. 307–316, 04 2010.

[2] R. Niiyama, S. Nishikawa, and Y. Kuniyoshi, "Athlete robot with applied human muscle activation patterns for bipedal running," in *IEEE-RAS Humanoids*, 2010, pp. 498–503.

[3] Y. Fukuoka *et al.*, "Pace running of a quadruped robot driven by pneumatic muscle actuators: An experimental study," *Applied Sciences*, vol. 12, no. 9, 2022.

[4] Q.-T. Dao and S.-i. Yamamoto, "Assist-as-needed control of a robotic orthosis actuated by pneumatic artificial muscle for gait rehabilitation," *Applied Sciences*, vol. 8, no. 4, 2018.

[5] T.-C. Tsai and M.-H. Chiang, "Design and control of a 1-dof robotic lower-limb system driven by novel single pneumatic artificial muscle," *Applied Sciences*, vol. 10, no. 1, 2020.

[6] H. T. Nguyen, V. C. Trinh, and T. D. Le, "An adaptive fast terminal sliding mode controller of exercise-assisted robotic arm for elbow joint rehabilitation featuring pneumatic artificial muscle actuator," *Actuators*, vol. 9, no. 4, 2020.

[7] H. Chi *et al.*, "Control of a rehabilitation robotic device driven by antagonistic soft actuators," *Actuators*, vol. 10, no. 6, 2021.

[8] D. Dragone *et al.*, "Design, computational modelling and experimental characterization of bistable hybrid soft actuators for a controllable-compliance joint of an exoskeleton rehabilitation robot," *Actuators*, vol. 11, no. 2, 2022.

[9] R. M. Robinson, C. S. Kothera, and N. M. Wereley, "Control of a heavy-lift robotic manipulator with pneumatic artificial muscles," *Actuators*, vol. 3, no. 2, pp. 41–65, 2014.

[10] J. T. Stoll, K. Schanz, and A. Pott, "Mechatronic control system for a compliant and precise pneumatic rotary drive unit," *Actuators*, vol. 9, no. 1, 2020.

[11] Y. Lin, Y.-X. Xu, and J.-Y. Juang, "Single-actuator soft robot for in-pipe crawling," *Soft Robotics*, vol. 10, no. 1, pp. 174–186, 2023.

[12] D. Caldwell, G. Medrano-Cerda, and M. Goodwin, "Braided pneumatic actuator control of a multi-jointed manipulator," in *IEEE SMC*, vol. 1, 1993, pp. 423–428 vol.1.

[13] M. Zinn *et al.*, "A new actuation approach for human friendly robot design," *The International Journal of Robotics Research*, vol. 23, no. 4-5, pp. 379–398, 2004.

[14] Z. Wang, Y. Torigoe, and S. Hirai, "A prestressed soft gripper: Design, modeling, fabrication, and tests for food handling," *IEEE Robotics and Automation Letters*, vol. 2, pp. 1909–1916, 2017.

[15] T. V. Minh *et al.*, "Modeling and control of a pneumatic artificial muscle manipulator joint – part i: Modeling of a pneumatic artificial muscle manipulator joint with accounting for creep effect," *Mechatronics*, vol. 22, no. 7, pp. 923–933, 2012.

[16] G. Andrikopoulos, G. Nikolakopoulos, and S. Manesis, "A survey on applications of pneumatic artificial muscles," in *2011 19th Mediterranean Conference on Control & Automation (MED)*, 2011, pp. 1439–1446.

[17] T. Goto *et al.*, "Characteristics verification of pneumatic artificial muscles for compressive loading," *Advanced Robotics*, vol. 37, no. 14, pp. 887–899, 2023.

[18] D. J. S. Ruth, J.-W. Sohn, K. Dhanalakshmi, and S.-B. Choi, "Control aspects of shape memory alloys in robotics applications: a review over the last decade," *Sensors*, vol. 22, no. 13, p. 4860, 2022.

[19] M. Tiboni *et al.*, "An innovative pneumatic mini-valve actuated by sma ni-ti wires: Design and analysis," *Proceedings of the Institution of Mechanical Engineers, Part I: Journal of Systems and Control Engineering*, vol. 225, pp. 443–451, 06 2011.

[20] M. Rimar *et al.*, "Pulse width modulation modeling for efficient pneumatic artificial muscle control," *Advances in Mechanical Engineering*, vol. 11, no. 12, p. 1687814019895439, 2019.

[21] M. Pipan and N. Herakovic, "Closed-loop volume flow control algorithm for fast switching pneumatic valves with pwm signal," *Control Engineering Practice*, vol. 70, pp. 114–120, 2018.

[22] B. Najjari *et al.*, "Position control of an electro-pneumatic system based on pwm technique and flc," *ISA Transactions*, vol. 53, no. 2, pp. 647–657, 2014.

[23] M. Taghizadeh, A. Ghaffari, and F. Najafi, "Modeling and identification of a solenoid valve for pwm control applications," *Comptes Rendus Mécanique*, vol. 337, no. 3, pp. 131–140, 2009.

[24] Q. Wang *et al.*, "Experimental analysis of new high-speed powerful digital solenoid valves," *Energy Conversion and Management*, vol. 52, no. 5, pp. 2309–2313, 2011.

[25] M. Stork, "Using pulse width modulation with carrier frequency changing for transmission of two separate signals," *Analog Integr. Circuits Signal Process.*, vol. 106, no. 3, p. 535–542, mar 2021.

[26] R. Burke, D. T. P. Levine, and F. Zajac, "Physiological types and histochemical profiles in motor units of the cat gastrocnemius," *The Journal of physiology*, vol. 234, pp. 723–48, 11 1973.

[27] J. Celichowski, M. Pogrzebna, and R. T. Raikova, "Analysis of the unfused tetanus course in fast motor units of the rat medial gastrocnemius muscle." *Archives Italiennes de Biologie*, vol. 143, no. 1, pp. 51–63, 2005.

[28] S. Davis and D. G. Caldwell, "pneumatic muscle actuators for humanoid applications - sensor and valve integration," in *IEEE-RAS Humanoids*, 2006, pp. 456–461.

[29] Z. Lertmanorat, K. Gustafson, and D. Durand, "Electrode array for reversing the recruitment order of peripheral nerve stimulation: Experimental studies," *Annals of biomedical engineering*, vol. 34, pp. 152–60, 02 2006.

[30] A. W. Monster and H. Chan, "Isometric force production by motor units of extensor digitorum communis muscle in man," *Journal of Neurophysiology*, vol. 40, no. 6, pp. 1432–1443, 1977.